Simplified Description of the Field Distribution in Finlines and Ridge Waveguides and Its Application to the Analysis of *E*-Plane Discontinuities

RAAFAT R. MANSOUR, MEMBER, IEEE, ROBERT S. K. TONG, MEMBER, IEEE, AND ROBERT H. MACPHIE, SENIOR MEMBER, IEEE

***Abstract*—Using closed-form equations for the field distribution of the eigenmodes in ridge waveguides, this paper presents a simplified analysis for ridge waveguide *E*-plane discontinuities. The accuracy of the calculated results is checked by comparison with experimental results. Closed-form equations are also presented for the field distribution of the dominant hybrid mode in unilateral and bilateral finlines. The usefulness of these equations in calculating the characteristic impedance and in determining the plane of the circularly polarized magnetic field in unilateral finlines is demonstrated.**

I. Introduction

FINLINE and ridge waveguide circuits have frequently been used in the design of microwave and millimeter-wave components that require single-mode broad-band operation. Such components usually incorporate different types of *E*-plane discontinuities. Over the past several years, various approaches [1]–[4] have been reported for the characterization of finline discontinuities. However, the great majority of these approaches were developed to treat structures with infinitely thin metallization thickness. Thus, they are not applicable to the analysis of ridge waveguide discontinuities.

More recently, two rigorous approaches have been reported for the characterization of ridge waveguide *E*-plane discontinuities [5], [6]. The first one [5] uses the spectral-domain technique and has the advantage of high numerical efficiency. It is, however, limited to structures with infinitely thin ridges. The second approach [6] applies the mode-matching technique and requires the determination of the field distribution of the ridge waveguide eigenmodes. In this approach, however, the field distribution of the TE and TM modes in the ridge waveguide is obtained by following the conventional method of solving the boundary value problem first for the eigenvalue (the propagation constant), then for the associated eigenvector. Besides its complexity, the computational effort involved in this approach is extremely large.

On the other hand, approximate closed-form equations for the field distribution of the TE modes in ridge waveguides have been reported in [7]. These equations have been also used with the variational technique in [8] to analyze slot resonators. However, due to the coupling between TE and TM modes, formulation of the scattering matrix of the ridge waveguide discontinuity requires a knowledge of the field distribution of both TE and TM modes.

In this paper, we present closed-form equations for the field distribution of the TM modes in ridge waveguides. The closed-form equations for both TE and TM modes are then used with the conservation of complex power technique [9] to provide an efficient analysis of ridge waveguide *E*-plane discontinuities. The validity of this analysis is verified by comparing our results with published results as well as experimental results.

Although numerous closed-form equations have been reported in the literature [10], [11] for calculating the propagation constant in finlines, no paper has appeared for quick and easy evaluation of the field distribution. In this paper, we also present closed-form equations for the field distribution for the dominant mode in unilateral and bilateral finlines. In addition to the practical usefulness of these equations in the design of nonreciprocal finline components [12], these equations can also be used to derive a closed-form expression for the characteristic impedance.

II. Field Description in Ridge Waveguides

The major complexity in formulating the scattering matrix of the discontinuity shown in Fig. 1 is in determining the field distribution of the eigenmodes in the ridge waveguide region. The propagation constants of the eigenmodes in ridge waveguides are related to the cutoff frequencies, which can be easily calculated according to [9]. With the assumption of a single term in the ridge gap (region II) of Fig. 2 and N expansion terms in the trough region (region I), and with the application of the boundary conditions on

Manuscript received April 11, 1988; revised August 17, 1988.
R. R. Mansour and R. S. K. Tong are with COM DEV Ltd., Cambridge, Ont., Canada N1R 7H6.
R. H. MacPhie is with the Department of Electrical Engineering, University of Waterloo, Waterloo, Ont., Canada N2L 3G1.
IEEE Log Number 8824203.

0018-9480/88/1200-1825$01.00

the tangential fields at $x=l$, the field distribution of the TE and TM modes can be written as

TE modes:

$$\vec{E}_{\mathrm{I}} = \sum_{n=0,1,2\cdots}^{N} A_n \left[\frac{n\pi}{b} \cos\alpha_n x \sin\frac{n\pi}{b} y \vec{a}_x - \alpha_n \sin\alpha_n x \cos\frac{n\pi}{b} y \vec{a}_y \right] e^{-j\beta z} \tag{1a}$$

$$\vec{H}_{\mathrm{I}} = \sum_{n=0,1,2\cdots}^{N} A_n \frac{\beta}{\omega\mu} \left[\alpha_n \sin\alpha_n x \cos\frac{n\pi}{b} y \vec{a}_x + \frac{n\pi}{b} \cos\alpha_n x \sin\frac{n\pi}{b} y \vec{a}_y + \frac{k_c^2}{j\beta} \cos\alpha_n x \cos\frac{n\pi}{b} y \vec{a}_z \right] e^{-j\beta z} \tag{1b}$$

$$\vec{E}_{\mathrm{II}} = \cos k_c \left(\frac{a}{2} - x \right) \vec{a}_y e^{-j\beta z} \tag{1c}$$

$$\vec{H}_{\mathrm{II}} = -\frac{\beta}{\omega\mu} \left[\cos k_c \left(\frac{a}{2} - x \right) \vec{a}_x + \frac{k_c}{j\beta} \sin k_c \left(\frac{a}{2} - x \right) \vec{a}_z \right] e^{-j\beta z} \tag{1d}$$

where

$$A_n = \frac{-\Gamma_n \cos(k_c s/2)}{\alpha_n \sin(\alpha_n l)(n\pi)} \left[\sin\frac{n\pi}{b}(h+d) - \sin\frac{n\pi}{b} h \right] \tag{1e}$$

$\Gamma_n = 1$ for $n=0$ and $\Gamma_n = 2$ for $n = 1,2,3\cdots$.

TM modes:

$$\vec{E}_{\mathrm{I}} = \sum_{n=1,2,3\cdots}^{N} B_n \left[\alpha_n \cos\alpha_n x \sin\frac{n\pi}{b} y \vec{a}_x + \frac{n\pi}{b} \sin\alpha_n x \cos\frac{n\pi}{b} y \vec{a}_y - \frac{k_c^2}{j\beta} \sin\alpha_n x \sin\frac{n\pi}{b} y \vec{a}_z \right] e^{-j\beta z} \tag{2a}$$

$$\vec{H}_{\mathrm{I}} = \sum_{n=1,2,3\cdots}^{N} B_n \frac{\omega\epsilon}{\beta} \left[-\frac{n\pi}{b} \sin\alpha_n x \cos\frac{n\pi}{b} y \vec{a}_x + \alpha_n \cos\alpha_n x \sin\frac{n\pi}{b} y \vec{a}_y \right] e^{-j\beta z} \tag{2b}$$

$$\vec{E}_{\mathrm{II}} = \left[\gamma \sin\gamma \left(\frac{a}{2} - x \right) \sin\frac{\pi}{d}(y-h) \vec{a}_x + \frac{\pi}{d} \cos\gamma \left(\frac{a}{2} - x \right) \cos\frac{\pi}{d}(y-h) \vec{a}_y - \frac{k_c^2}{j\beta} \cos\gamma \left(\frac{a}{2} - x \right) \sin\frac{\pi}{d}(y-h) \vec{a}_z \right] e^{-j\beta z} \tag{2c}$$

$$\vec{H}_{\mathrm{II}} = \frac{\omega\epsilon}{\beta} \left[-\frac{\pi}{d} \cos\gamma \left(\frac{a}{2} - x \right) \cos\frac{\pi}{d}(y-h) \vec{a}_x + \gamma \sin\gamma \left(\frac{a}{2} - x \right) \sin\frac{\pi}{d}(y-h) \vec{a}_y \right] e^{-j\beta z} \tag{2d}$$

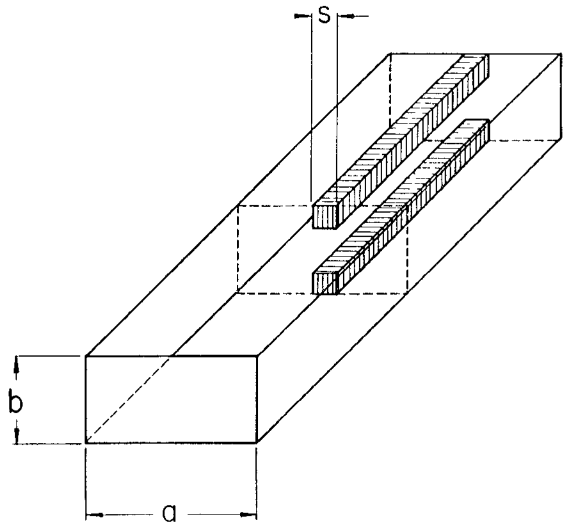

Fig. 1. Ridge waveguide E-plane discontinuity.

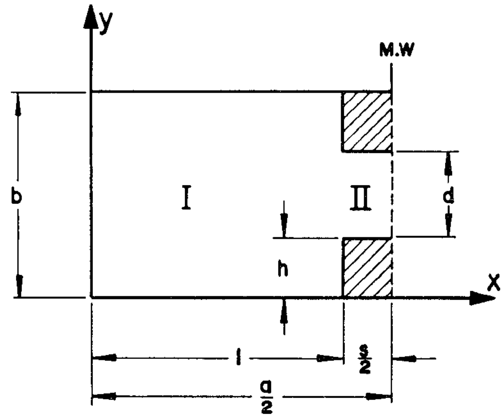

Fig. 2. Ridge waveguide with magnetic wall symmetry.

where

$$B_n = \frac{(\pi/d) 2\cos(\gamma s/2)}{b \sin\alpha_n l \left[(\pi/d)^2 - (n\pi/b)^2 \right]} \cdot \left[\sin\frac{n\pi}{b}(h+d) + \sin\frac{n\pi}{b} h \right]. \tag{2e}$$

The quantities β, k_c and γ are related as

$$\beta^2 = k_0^2 - k_c^2 \qquad k_c = 2\pi/\lambda_c$$

$$\alpha_n^2 = k_c^2 - \left(\frac{n\pi}{b} \right)^2 \qquad \gamma^2 = k_c^2 - \left(\frac{\pi}{d} \right)^2.$$

Equations (1) and (2) not only give the field distribution of the dominant TE mode and dominant TM mode. They also can be used to represent that of the higher order modes. It should, however, be mentioned that due to the use of a single expansion term (i.e., one mode) in the ridge gap, these equations may not accurately describe the fields near the edge of the ridge, but they provide a reasonable description elsewhere. The validity of (1) and (2) will be verified in Section III. A simple check of the validity of this procedure can, however, be achieved by comparing the ridge waveguide impedance calculated from these equa-

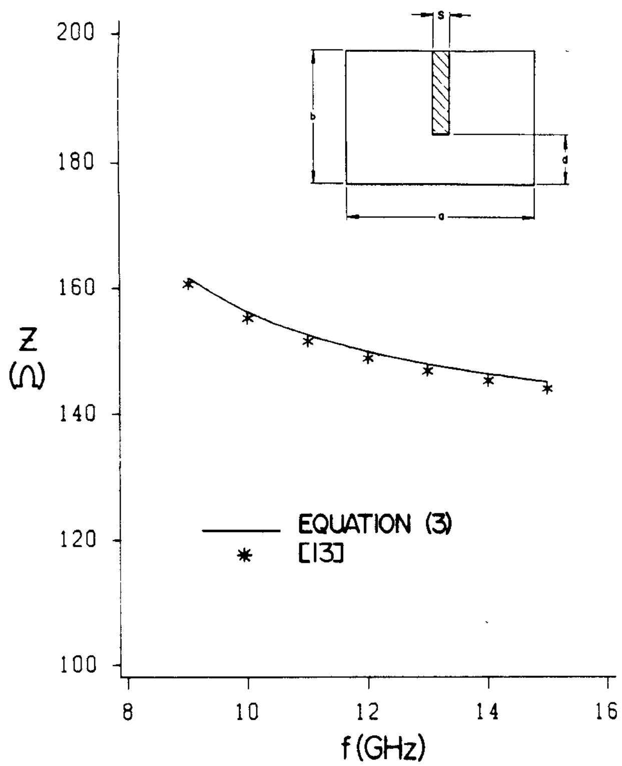

Fig. 3. Characteristic impedance versus frequency in ridge waveguide: $a = 19.0$ mm, $b = 8.55$ mm, $s = 0.3$ mm, $d = 1.7$ mm.

tions with other available data. The dominant mode characteristic impedance may be defined as

$$Z = \frac{V^2}{2P} = \frac{d^2}{2P} \tag{3a}$$

where V is the voltage across the ridge gap, d is the gap width, and P is the power propagation in the z direction, which can be written as

$$P = \frac{1}{2} \operatorname{Re} \int \vec{E} \times \vec{H}^* \cdot \vec{a}_z \, ds. \tag{3b}$$

Substituting (1) into (3b) gives

$$P = \frac{\beta}{2\omega\mu}\left[\sum_{n=1,2,3\cdots}^{N} |A_n|^2 \left(\frac{n\pi}{b}\right)^2 \frac{b}{\Gamma_n}\left[\frac{l}{2} + \frac{\sin 2\alpha_n l}{4\alpha_n}\right] + \sum_{n=0,1,2,\cdots}^{N} |A_n|^2 |\alpha_n|^2 \frac{b}{\Gamma_n}\left[\frac{l}{2} - \frac{\sin 2\alpha_n l}{4\alpha_n}\right] + d\left[\frac{S}{4} - \frac{\sin k_c S}{4k_c}\right]\right]. \tag{3c}$$

Fig. 3 illustrates a comparison between the characteristic impedance calculated from the closed-form expression given in (3) and that obtained using the variational technique [13]. It is noted that there is a good agreement.

III. Analysis of E-Plane Ridge Waveguide Discontinuities

The ridge waveguide discontinuity shown in Fig. 1 represents the basic building block in the design of many microwave and millimeter-wave components, among them

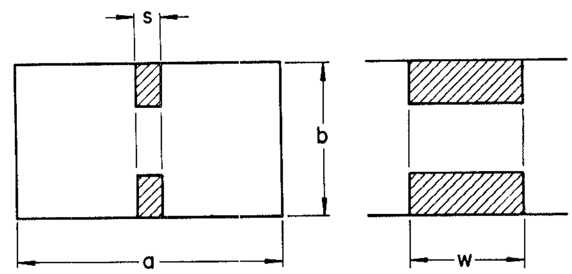

Fig. 4. Cascaded ridge waveguide E-plane discontinuity.

transformers [6] and evanescent mode filters [14]. Having determined the field distribution of the eigenmodes in ridge waveguides, the conservation of complex power technique [9] can then be employed to evaluate the scattering matrix of the ridge waveguide discontinuity. In view of [9], the scattering parameters may be written as

$$S_{22} = \left(P_2^\dagger + H^\dagger P_1^\dagger H\right)^{-1}\left(P_2^\dagger - H^\dagger P_1^\dagger H\right) \tag{4a}$$

$$S_{12} = H(I + S_{22}) \tag{4b}$$

$$S_{21} = 2\left(P_2^\dagger + H^\dagger P_1^\dagger H\right)^{-1} H^\dagger P_1^\dagger \tag{4c}$$

$$S_{11} = HS_{21} - I \tag{4d}$$

where † denotes Hermitian transpose. H is the E-field mode-matching matrix, which can be divided into four submatrices:

$$H = \begin{bmatrix} A & B \\ C & D \end{bmatrix}. \tag{5}$$

The submatrices A and D give the coupling between the TE and TM modes in the rectangular waveguide and the hybrid TE and TM modes in the ridge waveguide, whereas B and C indicate the cross-coupling between the modes in the two guides. P_1 and P_2 are diagonal matrices whose diagonal elements represent the power carried by unit amplitude modes in the rectangular and ridge waveguide, respectively. With the use of the generalized matrix technique [9], the overall scattering matrix of the cascaded ridge waveguide discontinuity shown in Fig. 4 can easily be evaluated.

In order to check the validity of this analysis, we compare in Fig. 5 our results with those reported in [5] using the spectral-domain technique. A good agreement is observed. Fig. 6 also shows a comparison between our results and experimental results for a structure with a ridge of finite metallization thickness. It is noted that there is a good agreement between the computed and the experimental results. The numerical results shown in Figs. 5 and 6 were obtained using (20 TE modes + 10 TM modes) in the rectangular waveguide and (eight TE modes + four TM modes) in the ridge waveguide.

In contrast to the variational technique used in [15], the effect of the higher order mode coupling can be taken into account in the present analysis. This in turn allows cascaded discontinuities to be accurately analyzed. Fig. 7 shows the transmission coefficient of two E-plane discontinuities connected in cascade. It is observed that the calculated results agree with the measured results.

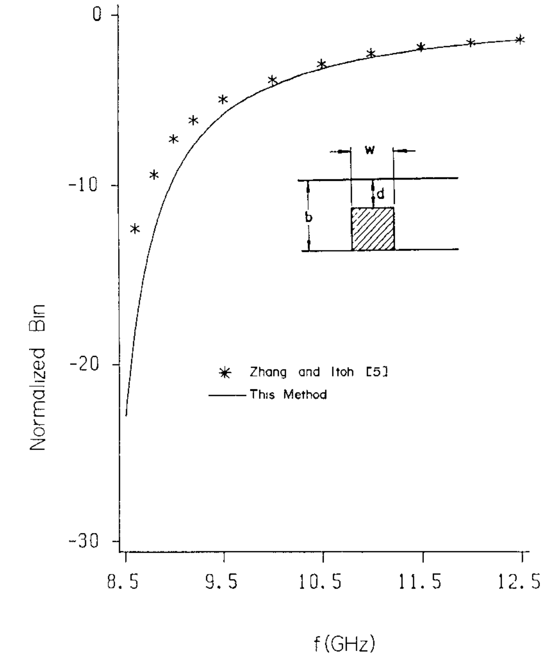

Fig. 5. Normalized susceptance of an E-plane ridge waveguide discontinuity: $a = 22.86$ mm, $b = 10.16$ mm, $h = 0.0$, $S = 0.0$, $l = 11.43$ mm, $d = 2.79$ mm, $w = 1.7$ mm.

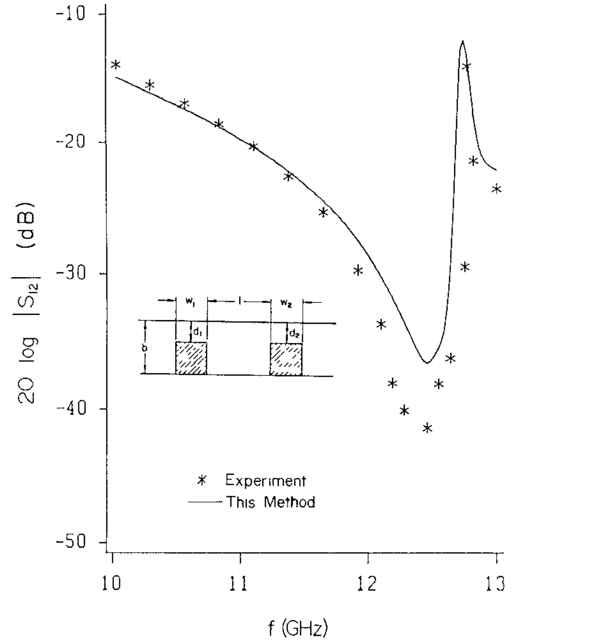

Fig. 7. Magnitude of transmission coefficient of a cascaded E-plane ridge waveguide discontinuity: $a = 22.86$ mm, $b = 10.16$ mm, $h = 0.0$, $S = 2.057$ mm, $l = 10.40$ mm, $d_1 = d_2 = 4.114$ mm, $l' = 12.192$ mm, $w_1 = w_2 = 1.524$.

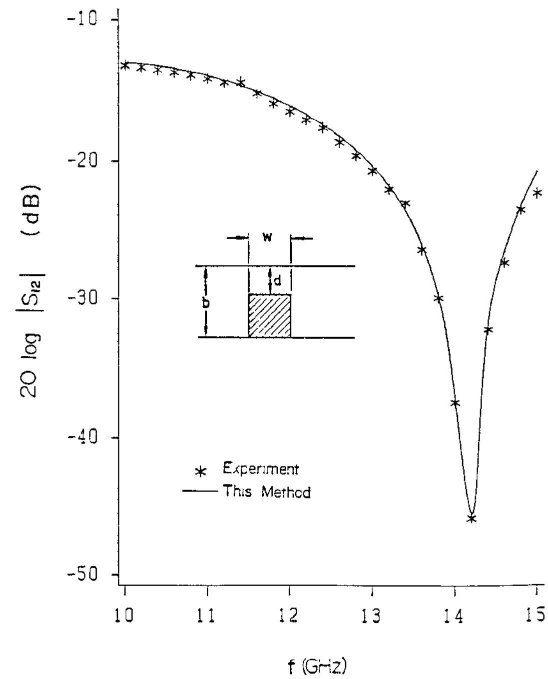

Fig. 6. Magnitude of transmission coefficient of an E-plane ridge waveguide discontinuity: $a = 19.05$ mm, $b = 9.524$ mm, $h = 0.0$, $S = 1.016$ mm, $l = 9.017$ mm, $d = 1.905$ mm, $w = 5.08$ mm.

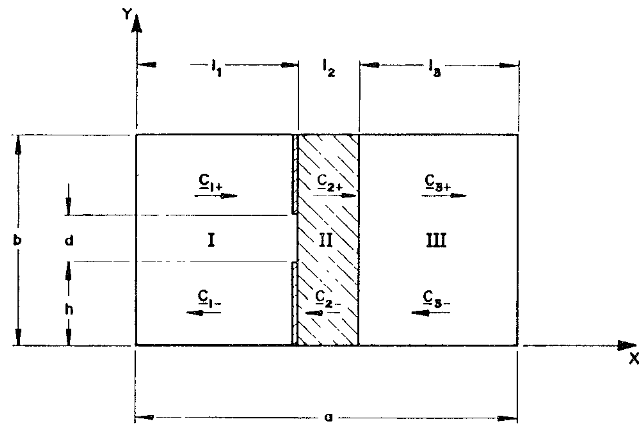

Fig. 8. A unilateral finline structure.

IV. Field Description in Unilateral Finlines

Due to the hybrid nature of the electromagnetic field in unilateral finlines, the field distribution is expressed as a summation of LSE and LSM modes. The propagation constant can be calculated using the closed-form expressions given in [10]. To demonstrate how the amplitudes of the LSE and LSM modes are determined, consider the unilateral finline structure shown in Fig. 8. Let the incident and reflected E-field mode amplitude vectors in regions I, II, and III be respectively presented by $\underline{C}\mathrm{R}_{i+}$ and $\underline{C}_{i-}$ ($i = 1$, 2 and 3). With the assumption of a constant field in the fin gap, continuity of the tangential field at $x_1 = l_1$ and $x_2 = l_1 + l_2$ gives

$$[\underline{C}_{1+}]_{x_1} + [\underline{C}_{1-}]_{x_1} = \boldsymbol{M} \tag{6a}$$

$$[\underline{C}_{2+}]_{x_1} + [\underline{C}_{2-}]_{x_1} = \boldsymbol{M} \tag{6b}$$

$$[\underline{C}_{2+}]_{x_2} + [\underline{C}_{2-}]_{x_2} = \left[[\underline{C}_{3+}]_{x_2} + [\underline{C}_{3-}]_{x_2}\right] \tag{6c}$$

where $\boldsymbol{M}$ is a column matrix whose elements represent the coupling between the modes in region I and the constant field in the fin gap. The amplitude vectors $\underline{C}_{i+}$ and $\underline{C}_{i-}$

are also related by

$$[\underline{C}_{1+}]_{x_1} = -L_1 L_1 [\underline{C}_{1-}]_{x_1} \tag{7a}$$

$$[\underline{C}_{2+}]_{x_2} = L_2 [\underline{C}_{2+}]_{x_1} \tag{7b}$$

$$[\underline{C}_{2-}]_{x_1} = L_2 [\underline{C}_{2-}]_{x_2} \tag{7c}$$

$$[\underline{C}_{2-}]_{x_2} = S [\underline{C}_{2+}]_{x_2} \tag{7d}$$

$$[\underline{C}_{3-}]_{x_2} = -L_3 L_3 [\underline{C}_{1+}]_{x_2} \tag{7e}$$

where L_i ($i = 1$, 2, and 3) are diagonal matrices with diagonal elements given by $L_{i,nn} = e^{-j\alpha_n l_i}$. The matrix S is a diagonal matrix whose elements can be derived according to [16, ch. 6]. Manipulating (6) and (7) gives the amplitudes of the LSE and LSM modes in regions I, II, and III. The field distribution of the dominant mode can then be approximated as follows:

$$\vec{E} = \vec{E}^h + \vec{E}^e \qquad \vec{H} = \vec{H}^h + \vec{H}^e$$

$$\vec{E}^h = \sum_{n=0,1,2\cdots}^{N} A_n \left[j\beta\phi_n(x)\cos\frac{n\pi}{b}y\vec{a}_y - \frac{n\pi}{b}\phi_n(x)\sin\frac{n\pi}{b}y\vec{a}_z \right] e^{-j\beta z} \tag{8a}$$

$$\vec{E}^e = \sum_{n=1,2,3\cdots}^{N} B_n \left[\frac{K_{cn}^2}{j\alpha_n}\Psi_n(x)\sin\frac{n\pi}{b}y\vec{a}_x + \frac{n\pi}{b}\phi_n(x)\cos\frac{n\pi}{b}y\vec{a}_y - j\beta\phi_n(x)\sin\frac{n\pi}{b}y\vec{a}_z \right] e^{-j\beta z} \tag{8b}$$

$$\vec{H}^h = \sum_{n=1,2,3\cdots}^{N} A_n \frac{\alpha_n}{\omega\mu} \left[\frac{K_{cn}^2}{j\alpha_n}\phi_n(x)\cos\frac{n\pi}{b}y\vec{a}_x - \frac{n\pi}{b}\Psi_n(x)\sin\frac{n\pi}{b}y\vec{a}_y - j\beta\Psi_n(x)\cos\frac{n\pi}{b}y\vec{a}_z \right] e^{-j\beta z} \tag{9a}$$

$$\vec{H}^e = \sum_{n=0,1,2\cdots}^{N} B_n \frac{\omega\epsilon}{\alpha_n} \left[-j\beta\Psi_n(x)\sin\frac{n\pi}{b}y\vec{a}_y - \frac{n\pi}{b}\Psi_n(x)\cos\frac{n\pi}{b}y\vec{a}_z \right] e^{-j\beta z} \tag{9b}$$

where A_n, B_n, ϕ_n, and Ψ_n are below for the various regions.

Region I (Unilateral Finline)

$$\phi_n(x) = j\sin\alpha_{1n}x \qquad \Psi_n(x) = \cos\alpha_{1n}x$$

$$A_n = \frac{-2j\beta W_n}{[e^{+j\alpha_{1n}l_1} - e^{-j\alpha_{1n}l_1}]} \qquad B_n = \frac{2(n\pi/b)W_n}{[e^{+j\alpha_{1n}l_1} - e^{-j\alpha_{1n}l_1}]}$$

$$W_n = \frac{\Gamma_n}{n\pi}\frac{1}{K_{cn}^2}\left[\sin\frac{n\pi}{b}(h+d) - \sin\frac{n\pi}{b}h\right].$$

Region II (Unilateral Finline)

$$\phi_n(x) = \left[S_n e^{+j\alpha_{2n}(x-l_1)} + e^{-j\alpha_{2n}(x-l_1)}\right]$$

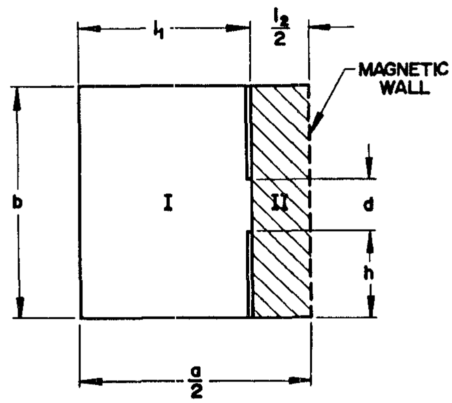

Fig. 9. A bilateral finline structure with magnetic wall symmetry.

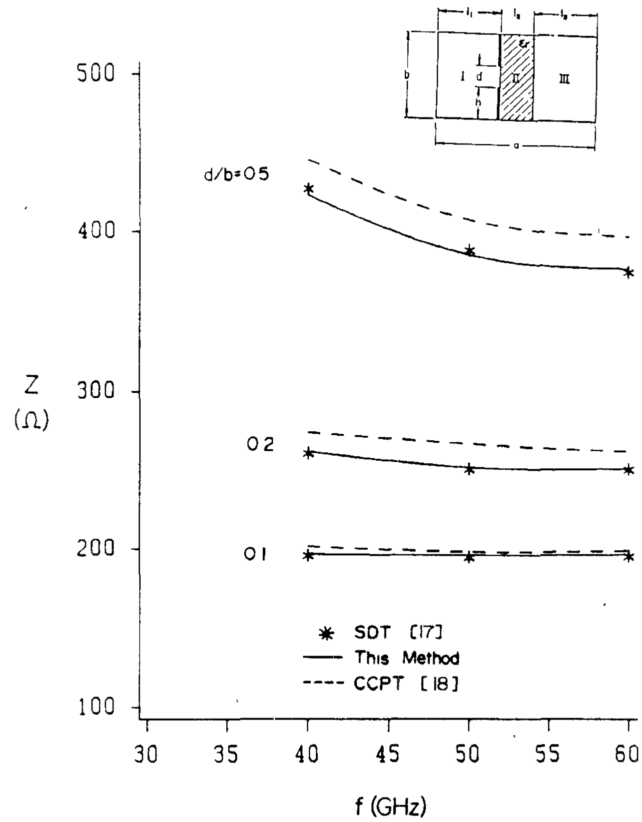

Fig. 10. Characteristic impedance versus frequency in unilateral finlines: $a = 2b = 4.7752$ mm, $l_2 = 0.127$ mm, $l_1 = 2.3876$ mm, $\epsilon_r = 2.2$.

$$\Psi_n(x) = \left[S_n e^{+j\alpha_{2n}(x-l_1)} - e^{-j\alpha_{2n}(x-l_1)}\right]$$

$$A_n = -j\beta\frac{W_n}{(1+S_n)} \qquad B_n = \frac{n\pi}{b}\frac{W_n}{(1+S_n)}$$

$$S_n = e^{-j2\alpha_{2n}l_2}\cdot\frac{(1-C_n)-(1+C_n)e^{-j2\alpha_{3n}l_3}}{(1+C_n)-(1-C_n)e^{-j2\alpha_{3n}l_3}}$$

$$C_n = \frac{\alpha_{3n}^*}{\alpha_{2n}^*} \qquad \text{for LSE modes}$$

$$C_n = \frac{\alpha_{2n}^*}{\epsilon_r\alpha_{3n}^*} \qquad \text{for LSM modes.}$$

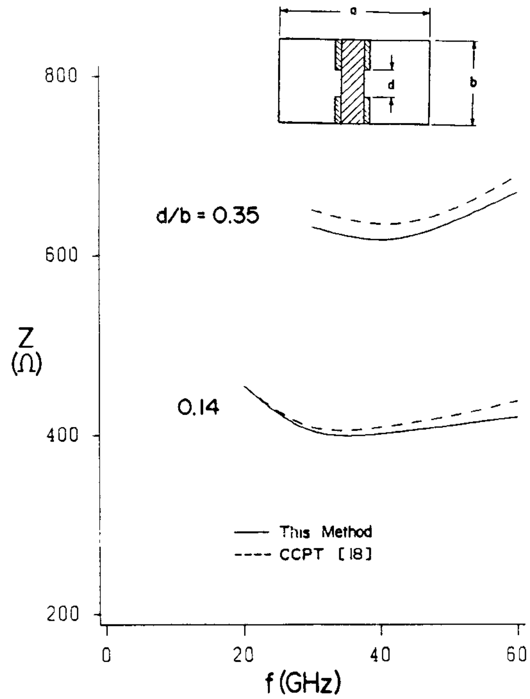

Fig. 11. Characteristic impedance versus frequency in bilateral finlines: $a = 2b = 7.112$ mm, $l_2 = 0.125$ mm, $\epsilon_r = 3.0$.

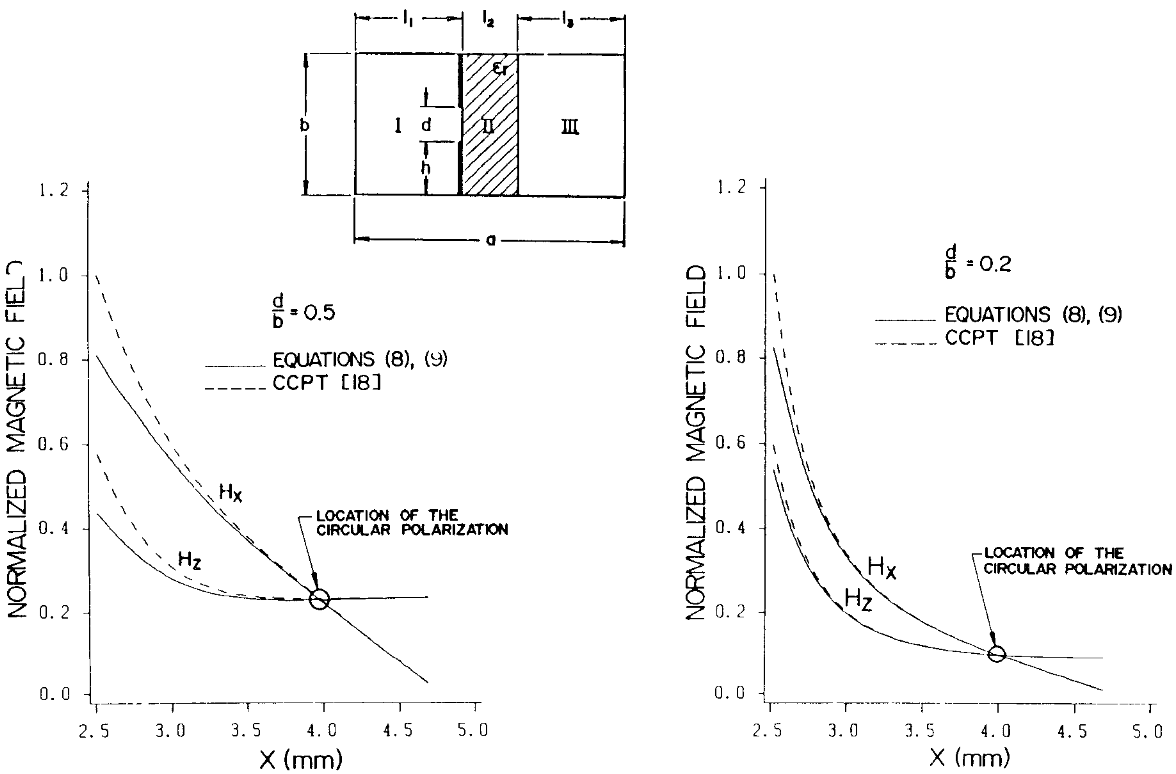

Fig. 12. The normalized magnetic field components in unilateral finlines: $a = 2b = 4.7752$ mm, $l_2 = 0.127$ mm, $l_1 = 2.3876$ mm, $\epsilon_r = 2.2$.

Region III (Unilateral Finline)

$$\phi_n(x) = j\sin\alpha_{3n}(x-a) \qquad \Psi_n(x) = \cos\alpha_{3n}(x-a)$$

$$A_n = -2j\beta W_n Y_n \qquad B_n = 2\frac{n\pi}{b}W_n Y_n$$

$$Y_n = \frac{\left[e^{-j\alpha_{2n}l_2} + e^{j\alpha_{2n}l_2}S_n\right]}{\left[e^{-j\alpha_{3n}l_3} - e^{+j\alpha_{3n}l_3}\right]\left[1+S_n\right]}$$

where

$$\Gamma_n = 1 \text{ for } n = 0 \text{ and } \Gamma_n = 2 \text{ for } n = 1,2,3\cdots$$

$$K_{cn}^2 = \left(\frac{n\pi}{b}\right)^2 + \beta^2 \qquad \alpha_{in}^2 = k_0^2\epsilon_{ri} - K_{cn}^2.$$

For bilateral finlines, due to symmetry around the x axis we only need to consider regions I and II, as shown in Fig. 9. The field distribution in region I is similar to that described in region I of the unilateral finline structure shown in Fig. 8. In region II, however, A_n, B_n ϕ_n and Ψ_n are given as follows.

Region II (Bilateral Finline)

$$\phi_n(x) = \cos\alpha_n\left(x - \frac{a}{2}\right) \qquad \Psi_n(x) = j\sin\alpha_n\left(x-\frac{a}{2}\right)$$

$$A_n = -j\beta W_n Y_n \qquad B_n = \frac{n\pi}{b}W_n Y_n$$

$$Y_n = \frac{e^{-j\alpha_{2n}l_2/2}}{\left[1+e^{-j\alpha_{2n}l_2}\right]}.$$

Having obtained the E and H field components, the characteristic impedance can be evaluated as demonstrated in Section II. In Fig. 10 we compare the characteristic impedance of unilateral finlines calculated using (8) and (9) with those reported in [17] using the spectral-domain technique. It is noted that there is a good agreement. It should, however, be mentioned that in [17] a constant field is also assumed in the fin gap. In order to verify the validity of (8) and (9), Fig. 10 also shows results calculated using the more exact analysis reported in [18]. Good agreement is observed when d/b is relatively small. Similar results were also obtained for bilateral finlines, as illustrated in Fig. 11.

Another useful application of (8) and (9) is in determining the plane of the pure circularly polarized magnetic field in unilateral finlines, which is needed in the design of finline isolators [12]. Fig. 12 shows a comparison between the normalized magnetic field components for a wave propagating in the positive z direction calculated using (8) and (9) and those obtained using the rigorous analysis [18]. The location of the plane of the circularly polarized magnetic field is also illustrated in this figure for the two cases of $d/b = 0.2$ and $d/b = 0.5$.

It is concluded from Figs. 6, 7, 10, 11, and 12 that (1), (2), (8), and (9) can reasonably well approximate the field distribution in structures with relatively small gap sizes ($d/b < 0.2$). This is, however, the case in most practical applications.

V. Conclusions

Novel closed-form equations are reported for the field distribution of TM modes in ridge waveguides as well as the dominant mode in unilateral and bilateral finlines. Numerical results are presented which confirm the usefulness of these equations in calculating the characteristic impedance and determining the location of the circularly polarized magnetic field in unilateral finlines. The use of these equations in achieving a simplified analysis of E-plane ridge waveguide discontinuities has been demonstrated. The numerical results obtained for different discontinuities agree well with the experimental data.

Acknowledgment

The authors express their sincere thanks to Dr. C. Kudsia for his valuable comments on the work and to the management of COM DEV Ltd. for permission to publish the work. They would like also to thank H. Gabert and V. Dokas for preparing the experimental data.

References

[1] J. Knorr, "Equivalent reactance of a shorting septum in a finline: Theory and experiment," *IEEE Trans. Microwave Theory Tech.*, vol. MTT-29, pp. 1196–1202, Nov. 1981.

[2] R. Sorrentino and T. Itoh, "Transverse resonance analysis of finline discontinuities," *IEEE Trans. Microwave Theory Tech.*, vol. MTT-32, pp. 1633–1638, Dec. 1984.

[3] M. Helard, J. Citerne, O. Picon and V. Hanna, "Theoretical and experimental investigation of finline discontinuities," *IEEE Trans. Microwave Theory Tech.*, vol. MTT-33, pp. 994–1003, Oct. 1985.

[4] K. Webb and R. Mittra, "Solution of the finline step discontinuity problem using the generalized variational technique," *IEEE Trans. Microwave Theory Tech.*, vol. MTT-33, pp. 1004–1010, Oct. 1985.

[5] Q. Zhang and T. Itoh, "Spectral domain analysis of scattering from *E*-plane circuit elements," *IEEE Trans Microwave Theory Tech.*, vol. MTT-35, pp. 138–150, Feb. 1987.

[6] J. Bornemann and F. Arndt, "Modal *S*-matrix design of optimum stepped ridged and fined waveguide transformers," *IEEE Trans. Microwave Theory Tech.*, vol. MTT-35, pp. 561–567, June 1987.

[7] W. J. Getsinger, "Ridged waveguide field description and application to directional couplers," *IRE Trans Microwave Theory Tech.*, vol. MTT-10, pp. 41–50, Jan. 1962.

[8] Y. Konishi and H. Matsumura, "Short end effect of ridge guide with planar circuit mounted in a waveguide," *IEEE Trans. Microwave Theory Tech*, vol. MTT-27, pp. 168–170, Feb 1979.

[9] R. R Mansour and R. H. MacPhie, "An improved transmission matrix formulation of cascaded discontinuities and its application to *E*-plane circuits," *IEEE Trans. Microwave Theory Tech.*, vol. MTT-34, pp. 1490–1498, Dec 1986.

[10] P. Bhartia and P. Pramanick, *E-Plane Integrated Circuits*. Norwood, MA: Artech House, 1987.

[11] B. Bhat and S. Koul, *Analysis, Design and Applications of Finlines*. Norwood, MA: Artech House, 1987.

[12] A. Beyer and I. Wolf, "A finline isolator and circulator for *R*-band," in *Proc. European Microwave Conf.*, pp. 321–326, 1981.

[13] Y. Utsumi, "Variational analysis of ridged waveguide modes," *IEEE Trans. Microwave Theory Tech.*, vol. MTT-33, pp. 111–120, Feb. 1985

[14] Q. Zhang and T. Itoh, "Computer-aided design of evanescent-mode waveguide filter with nontouching *E*-plane fins," *IEEE Trans. Microwave Theory Tech.*, vol. MTT-36, pp. 404–412, Feb. 1988.

[15] K. Chang and P J. Khan, "Analysis of narrow capacitive strip in waveguides," *IEEE Trans Microwave Theory Tech.*, vol. MTT-22, pp. 536–541, May 1974.

[16] R. Collin, *Field Theory of Guided Waves*. New York: McGraw-Hill, 1960.

[17] J. B. Knorr and P. M. Shayda, "Millimeter-wave finline characteristics," *IEEE Trans. Microwave Theory Tech.*, vol. MTT-28, pp. 737–743, July 1980.

[18] R. R. Mansour and R. H. MacPhie, "A unified hybrid mode analysis of planar transmission lines with multilayer isotropic/anisotropic substrates," *IEEE Trans. Microwave Theory Tech.*, vol. MTT-35, pp. 1382–1391, Dec. 1987.

Raafat R. Mansour (S'84–M'86) was born in Cairo, Egypt, on March 31, 1955. He received the B.Sc (with honors) and M.Sc degrees from Ain Shams University, Cairo, in 1977 and 1981, respectively, and the Ph.D. degree from the University of Waterloo, Ont., Canada, in 1986, all in electrical engineering.

He was a research fellow at the Laboratoire d'Electromagnetisme, Institut National Polytechnique, Grenoble, France, in 1981. From 1983 to 1986 he was a Research and Teaching Assistant with the Department of Electrical Engineering, University of Waterloo. Since then he has been with COM DEV Ltd., Cambridge, Ont., Canada, where he is currently a Senior Member of the Technical Staff. His present research interests are in the analysis and design of microwave and millimeter-wave integrated circuits.

Dr. Mansour received the 1987 University of Waterloo Engineering award for outstanding achievement. He was also awarded a Natural Sciences and Engineering Research Council of Canada NSERC Fellowship in 1987.

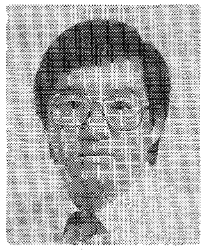

Robert S. K. Tong (M'85) was born in Hong Kong on June 1, 1959. He received the B.Eng degree (with honors) from McMaster University, Ont., Canada, in 1981 and the M.Sc. degree from the University of Waterloo, Ont., Canada, in 1988, both in electrical engineering.

In 1981, he joined COM DEV Ltd., Ont., Canada, as a Member of Technical Staff involved in the development of microwave filters and multiplexers for satellite applications. From 1984 to 1988, he was project manager in the COM DEV Satellite Division, responsible for the production of microwave multiplexer assemblies. Currently, he is Manager of EHF programs in the COM DEV Defense Division, responsible for the development of millimeter-wave active and passive components and millimeter-wave subsystems for defense applications.

Robert H. MacPhie (S'57–M'63–SM'79) was born in Weston, Ont., Canada, on September 20, 1934. He received the B.A.Sc. degree in electrical engineering from the University of Toronto in 1957 and the M.S. and Ph.D. degrees from the University of Illinois, Urbana, in 1959 and 1963, respectively.

In 1963, he joined the University of Waterloo, Waterloo, Ont., Canada, as an Assistant Professor of electrical engineering and at present he is Professor of electrical engineering at Waterloo. His research interests currently focus on dipole antennas, signal processing antenna systems, scattering from prolate spheroid systems, and microstrip structures. During the academic year 1984–1985, he was on sabbatical leave as a Professeur Associe at the Universite de Aix-Marseille, France, working in the Department de Radioelectricite.